machines

MDPI

Article

Research on Recognition Method for Typical Drilling Conditions Based on Drill Bit Motion Characteristics

Hang Chen [1,2,3], Qingfeng Wang [1,2,3], Mingyuan Sun [4], Dezhong Xin [1,2,3], Jianbo Dai [2,4,*], Zhongbin Wang [4], Lei Si [4] and Yan Zhang [4]

[1] China Coal Research Institute, Beijing 100013, China; 2010008@cqccteg.com (H.C.)
[2] State key Laboratory of Coal Mine Disaster Prevention and Control, Chongqing 400073, China
[3] CCTEG Chongqing Research Institute Co., Ltd., Chongqing 400039, China
[4] College of Mechanical and Electrical Engineering, China University of Mining and Technology, Xuzhou 221116, China
* Correspondence: jianbodai@cumt.edu.cn

Abstract

Drilling conditions serve as reliable indicators for evaluating drilling system performance. The recognition methodology forms a critical foundation for intelligent drilling and plays a significant role in preventing borehole accidents such as pipe sticking. This study proposes a recognition method for typical drilling conditions based on bit motion characteristics, developing intelligent algorithms that utilize fundamental motion parameters and drive signals as inputs to achieve accurate condition identification. Firstly, micro-drilling experiments were conducted under various pressure and rotational speed combinations. The variation characteristics of drilling speed, rotational speed, torque, and drilling pressure during the process were analyzed. Based on rotational and feed motion features at different stages, four typical drilling conditions were defined: stable drilling, slowing-down drilling, intermittent jamming, and pipe sticking. Subsequently, using actual coal mine drilling data, feature indicators for recognition models were selected through collective statistical characteristics and rolling statistical properties. Recognition models employing support vector machine (SVM), convolutional neural network (CNN), and long short-term memory (LSTM) networks were constructed and trained. Test results demonstrate that the LSTM-based model achieved the highest recognition accuracy (84% overall). It attained 100% accuracy in identifying slowing-down drilling and intermittent jamming conditions, though recognition accuracy for stable drilling remained relatively low. This research contributes to enhanced intelligent recognition of drilling conditions and provides theoretical support for advancing intelligent drilling technologies.

Keywords: drilling conditions recognition; drill bit motion characteristics; drilling speed; intelligent algorithms

Check for updates

Academic Editor: Angelos P. Markopoulos

Received: 23 December 2025
Revised: 1 February 2026
Accepted: 5 February 2026
Published: 9 February 2026

Copyright: © 2026 by the authors. Licensee MDPI, Basel, Switzerland. This article is an open access article distributed under the terms and conditions of the Creative Commons Attribution (CC BY) license.

1. Introduction

Drilling serves as a critical method for preventing and mitigating disasters such as gas and impact pressure in coal mine underground operations. With the advancement of intelligent coal mine construction and the deepening of the "unmanned means safety" philosophy, intelligent drilling equipment, including smart drilling rigs, drilling robots, and advanced proactive drilling solutions, has emerged in recent years [1–3]. The realization of autonomous drilling capabilities has become an inevitable path for coal mine drilling technology to evolve toward intelligent and unmanned operations [4]. Therefore, research

on adaptive control of drilling parameters is crucial for achieving unmanned drilling operations [5], with adaptive control methods for identifying typical drilling conditions serving as a fundamental basis.

Drilling conditions refer to the in-hole drilling state formed under the combined influence of factors such as the physical and mechanical properties of rock formations, the interaction between drilling tools and rock formations, and the fluid interactions between drill cuttings and drilling fluid [6]. These conditions reflect the operational status of the drilling system. As a complex and time-varying state, drilling conditions critically impact drilling efficiency, equipment condition, and even construction safety. Therefore, studying the changes in drilling conditions during the drilling process can provide effective evidence for safe, efficient, and intelligent drilling.

In the early stages of drilling technology development, operators primarily relied on manual data analysis to identify operational changes. They adjusted drilling parameters based on human experience when detecting anomalies, but this approach remained subjective and arbitrary, failing to accurately reflect real-world conditions. During the initial phase of intelligent drilling technology development, programming-based recognition methods emerged, incorporating classical condition models or human experience models. Wang [7] proposed a drilling condition perception method using boundary conditions such as stuck pipe probability, slag discharge smoothness, and anchoring stability. Although tested on drilling robots, this method still depended on programmed physical models and human experience. Zhang [8] identified borewell surges and leaks by combining parameter threshold judgments with condition selection, though the recognition process remained heavily reliant on human expertise. Wang [9] analyzed axial and cutting forces in typical coal bed drilling operations, establishing load variation correlations with four rock samples, but did not conduct in-depth data mining or intelligent training.

With the advancement of intelligent drilling technologies, artificial intelligence algorithms such as decision trees, support vector machines, and neural networks have been increasingly applied to drilling condition recognition. Rosiani [10] proposed an early warning system using support vector machine and artificial neural network models to predict and classify conditions as normal, pre-stuck, or stuck. The results showed that SVM could provide better prediction results than ANN, offering a fast and effective method for early detection by improving response times and accuracy in preventing stuck pipe incidents. Moving beyond threshold methods, Sun et al. [11] introduced a real-time recognition technique utilizing support vector machines (SVMs). Their work involved constructing an SVM model and comparing different kernel functions to optimize its parameters, thereby reducing the uncertainty and subjectivity associated with manual identification and increasing productive drilling time. Gao [12] divided the drilling conditions into standpipe connection, tripping out, tripping in, reaming, back reaming, circulation, drilling, and other conditions, and compared the accuracy of the integrated model and the base learner. The stacking model fusion method has a good recognition effect under the standpipe connection condition, tripping in condition, and drilling condition. For specific hazard detection, Du [13] conducted real-time diagnostic analysis of overflow risk by developing both BP neural network and Random Forest models, focusing on drilling parameters that exhibit significant changes during overflow events. In a different approach, Yin et al. [14] achieved intelligent identification of drilling operations by integrating mathematical statistics with manual empirical models. This identification formed the basis for a detailed division of daily and total operational time for drilling activities.

Utilizing actual drilling data, Wang [15] employed wavelet decomposition and reconstruction techniques to eliminate data; this approach was subsequently used to identify six standard drilling operational states through a hybrid algorithm combining a 1D con-

volutional neural network with a bidirectional generative adversarial network. Jared et al. [16] evaluated linear regression, quadratic Poisson regression, support vector machine regression, random forest, and gradient boosting to forecast small-sized unconventional reservoirs. It was found that a random forest-based stacking model delivered the highest prediction accuracy. For fluid identification in high-temperature, high-pressure reservoirs of the Yinggehai Basin, Qin et al. [17] constructed weak learners—decision trees, support vector machines, random forests, and GBDT—that demonstrated effective fluid identification, and fused using a stacking model fusion method to distinguish between dry layers, gas layers, gas–water layers, and water layers based on well-logging response characteristics. This fused model exhibited superior accuracy and robustness compared to any single model used in isolation. In well-kick risk prediction, Zhao et al. [18] preprocessed field data using the k-means clustering method for normalization and combined it with four different artificial neural network architectures. Their comparative analysis concluded that a model integrating a regularized radial basis function neural network (RBFNN) with k-means clustering achieved the highest prediction accuracy.

While significant research has been devoted to intelligent drilling condition recognition in petroleum engineering, its application to underground coal mine drilling systems remains relatively underexplored. These systems represent complex, time-varying environments that differ significantly from their petroleum counterparts in terms of geology, operational constraints, and scale. Consequently, analyzing actual underground coal mine drilling scenarios presents distinct challenges, compounded by the complexity of downhole conditions and the current limitations in precise sensing and control technologies for such specific applications.

To address this, this study establishes a miniature drilling experiment system based on similarity principles to simulate underground coal mine drilling operations. Through experimental analysis of evolving drilling characteristics under varying parameters, we identify typical drilling conditions by examining time-frequency domain features of process variables including drilling pressure, torque, and drilling speed. By comparing three distinct models—support vector machines (SVMs), convolutional neural networks (CNNs), and long short-term memory networks (LSTMs)—with actual underground drilling data, we evaluate their performance in recognizing typical drilling conditions. The optimized model demonstrates enhanced accuracy in identifying characteristic drilling scenarios, providing theoretical support for advancing intelligent drilling technologies in coal mining. The present research provides a critical and accurate method of identifying downhole drilling conditions in real time, which is beneficial for the realization of autonomous and intelligent drilling in underground coal mine operations.

2. Methodology

To simulate the drilling process for underground drilling rigs in coal mines, a miniature drilling test bench was employed to conduct experimental studies, yielding experimental data for theoretical research on drilling conditions. The experimental design is grounded in similarity theory [19], which ensures that the physical processes in the scaled-down model accurately represent those in the full-scale prototype. The core principle is to maintain consistency of key dimensionless parameters derived through dimensional analysis of the drilling mechanics. The primary assumption is the geometric, kinematic, and dynamic similarity of the rock fragmentation and tool interaction process. This approach ensures that the trends and relationships observed in the micro drilling experiment are qualitatively and quantitatively representative of real field drilling conditions. The test bench's fundamental geometric similarity coefficient is 1/10. The similarity coefficients of other relevant parameters, derived from the governing physical laws, are listed in Table 1.

Table 1. Similarity Coefficients of Parameters Related to Micro Drill Experiment.

Parameter	Similarity Factor
Borehole diameter/mm	1/10
Rotational speed/(r/min)	$\sqrt{10}$
Torque/(N·m)	1/10,000
Drilling pressure/N	1/1000
Feed rate/(m/min)	$1/\sqrt{10}$

The miniature drilling test bench consists of three core components: the drilling assembly, measurement system, and control unit (Figure 1). The drilling assembly includes an 8 mm diameter 8 mm twist drill bit, a rotary stepper motor, and a feed servo motor. During operation, the stepper motor drives the drill bit at 3000 rpm with 0.8 N m torque, while the servo motor supplies feed force at 2.4 N m torque. The experiment employs constant torque output from the servo motor to simulate continuous pressure drilling in automated rigs, with the drilling pressure calculated using Equation (1):

$$F = \frac{0.002\pi\eta T}{P_h} \tag{1}$$

where T denotes the torque of the servo motor (N·m), P_h represents the lead length of the feed screw (mm), and η indicates the mechanical efficiency of the feed screw transmission with a measured value of η = 0.9.

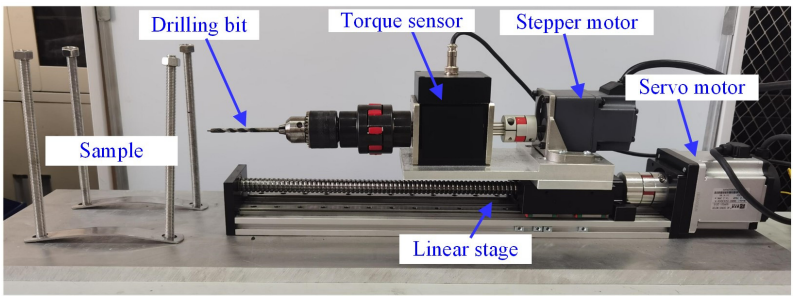


Figure 1. Micro drilling test platform.

In the measurement system, a torque sensor (model JN-3M1, manufactured by Bengbu Teluosen System Engineering Co., Ltd., Bengbu, China) is installed between the rotary motor and drill bit to monitor drilling torque and rotational speed in real time. The servo motor (Panasonic MSMT022S1D, manufactured by Panasonic Corporation, Osaka, Japan) provides real-time torque and speed readings, while measurement data from both stepper motors and servo motors are transmitted to the control computer via serial communication. The control system, comprising a Siemens S7-1200 programmable logic controller (PLC, manufactured by Siemens AG, Munich, Germany) and a data analysis computer, manages the operation of stepper and servo motors and collects operational data.

The experiment with constant drilling pressure and constant drilling speed was carried out by using the micro drilling test bench. The specimens were coal with a hardness of 2, a density of 1.35 g/cm^3, a uniaxial compressive strength (UCS) of 18.7 MPa, and an elastic modulus of 2.8 GPa. The micro drilling experiment was carried out with 5 different drilling pressures and 5 different drilling speeds, as shown in Table 2, and a total of 50 sets of drilling control parameters were tested.

Table 2. Drilling parameters.

Number	Drilling Pressure (N)	Rotational Speed (r/min)	Sample
1~50	62.8 93.2 125.6 157 188.4	250 500 750 1000 1250	Coal

3. Results

3.1. Characteristics of Stable Drilling

The variation of four parameters: drilling speed, torque, rotational speed, and drilling pressure at a set rotational speed of n = 750 r/min and drilling pressure F = 62.8 N is shown in Figure 2. As shown in Figure 2a, the drilling process can be divided into two main stages: the penetration stage and the steady drilling stage. During the period from 0 s to 1.95 s, since the stepper motor and servo motor have just started up and the drill bit has not yet contacted the specimen, the drill bit is unloaded, resulting in zero drilling torque, while the drilling speed increases rapidly. At t = 1.95 s, the drill bit contacts the specimen and encounters cutting resistance, causing the drilling speed to drop sharply from 1.62 mm/s to 1.25 mm/s. As the drill bit gradually penetrates the specimen, the torque increases approximately linearly, marking the penetration stage. At t = 15 s, the drilling torque reaches its maximum value and then stabilizes around 0.6 N m. Meanwhile, although the drilling speed slightly decreases compared to the penetration stage, it remains oscillating slightly around 1.1 mm/s. This stage is the steady drilling stage. As shown in Figure 2b, during the steady drilling stage, the drilling pressure remains almost unchanged, and the rotational speed oscillates only slightly around a steady value.

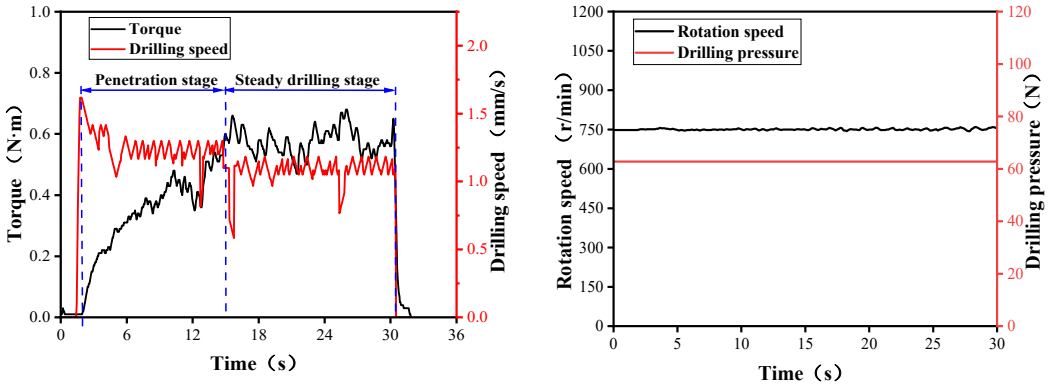


Figure 2. Variation of drilling parameters at steady state: (**a**) Variation of torque and drilling speed; (**b**) Variation of rotational speed and drilling pressure.

3.2. Characteristics of Slowing-Down Drilling

The variation curves for four parameters: torque, drilling speed, rotational speed, and drilling pressure under the conditions of rotational speed n = 250 r/min and drilling pressure F = 94.2 N are shown in Figure 3. As illustrated in Figure 3a, the drilling process can be divided into three main stages: the penetration stage, the steady drilling stage, and the drilling speed reduction stage. During the initial 0 s to 1.4 s period, the drill bit has not yet made contact with the specimen. At t = 1.4 s, the drill bit contacts the specimen, and torque begins to gradually increase while drilling speed decreases progressively with increasing depth, marking the penetration stage. At t = 5 s, the drill bit enters the steady drilling stage, where both torque and drilling speed oscillate toward stable values. By

t = 14 s, although torque stabilizes, drilling speed drops sharply to zero, indicating the speed reduction stage. Figure 3b shows that while rotational speed and drilling pressure remain relatively stable, at t = 16.25 s, torque oscillates around 0.25 N·m with significantly increased amplitude, reaching a minimum of 165 r/min, and continues to exhibit substantial oscillation throughout the subsequent phase.

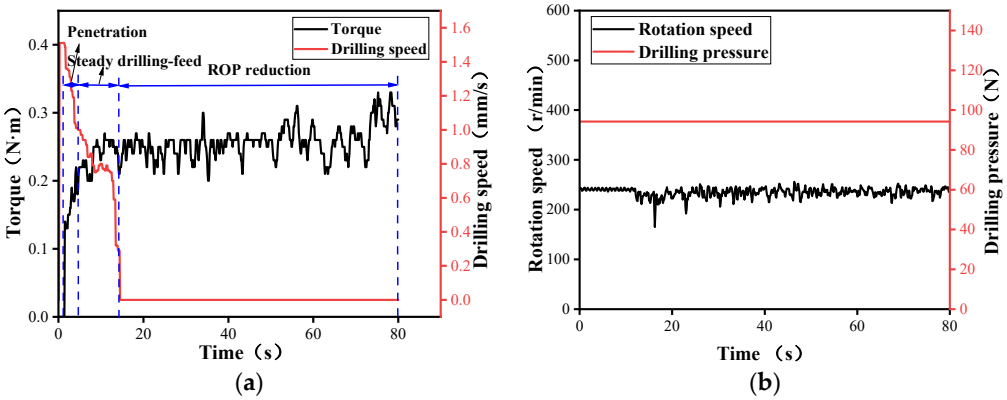


Figure 3. Variation of drilling parameters at slowing-down drilling state: (**a**) Variation of torque and drilling speed; (**b**) Variation of rotational speed and drilling pressure.

3.3. Characteristics of Intermittent Jamming and Pipe Sticking

Figure 4 displays the variation of four parameters (torque, drilling speed, rotational speed, and drilling pressure) at rotational speed n = 1250 r/min and drilling pressure F = 188.4 N. As shown in Figure 4a, the torque and rotational speed trends during the drilling phase and steady drilling phase are consistent with the steady state. At t = 4.6 s, the drilling torque surges from 0.7 N·m (steady state) to 0.95 N·m, while the drilling speed plummets from 1.03 mm/s to zero almost simultaneously, followed by sustained torque oscillations—this marks the intermittent jamming phase. Figure 4b reveals that during this phase, the drilling pressure remains near a steady value, whereas the rotational speed begins dramatic oscillations from t = 4.6 s, with a minimum of 0.

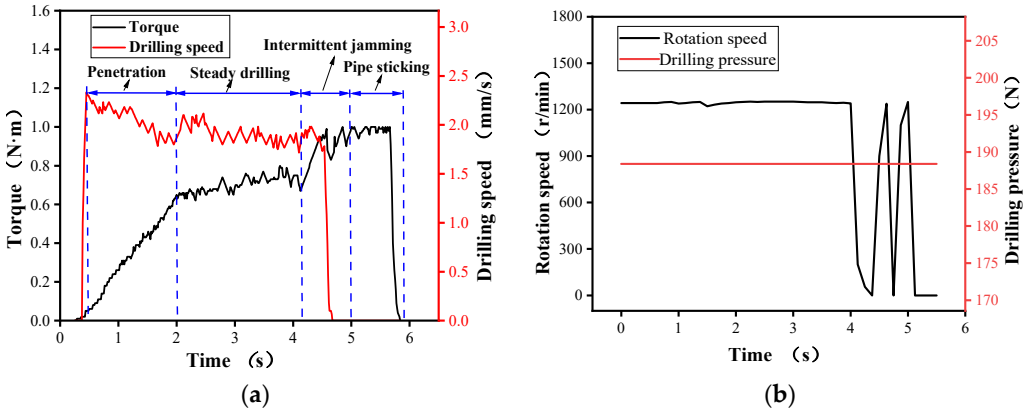


Figure 4. Variation of drilling parameters at intermittent stuck condition: (**a**) Variation of torque and drilling speed; (**b**) Variation of rotational speed and drilling pressure.

Compared with actual drilling conditions, intermittent jamming typically occurs before a large number of stuck bits appear, representing a transitional state between jamming and normal drilling. As shown in Figure 4a,b, the jamming state is defined when torque and feed pressure are continuously applied while drilling speed and rotational speed remain at zero (after 5 s).

3.4. Classification of Typical Drilling Conditions Based on Drilling Bit Motion

According to the motion characteristics of the drilling bit in this experiment, the drilling process can be defined as comprising four typical drilling states: stable drilling, slowing-down drilling, intermittent jamming, and pipe sticking, as shown in Table 3.

Table 3. Characteristics of different drilling states.

Drilling State	Class Label	Defining Condition	Key Parameter Variation
Stable drilling	0	Normal rotation and feed with minimal fluctuation.	v, n, T, F all maintained within ±15% of their mean steady-state values.
Slowing-down drilling	1	Significant and sustained decrease in penetration rate.	Drilling speed (v) decreases by >50% from its stable-stage average. Torque (T) may show minor fluctuation. Rotational speed (n) and pressure (F) remain relatively stable.
Intermittent jamming	2	Transient episodes of halted penetration and rotation.	v drops to near zero (<0.1 mm/s). T shows a sharp spike (>150% of prior stable value). n exhibits large, transient oscillations. F remains applied.
Pipe sticking	3	Complete cessation of drilling progress.	Drilling speed (v) = 0 mm/s. Rotational speed (n) = 0 rpm. Torque (T) remains at a constant, elevated value.

Stable Drilling: In this state, the bit maintains normal rotation and feed, with all drilling parameters (torque, drilling speed (v), rotational speed (n), and drilling pressure) fluctuating within a predetermined safe range, specifically within ±15% of their mean steady-state values. This state represents the highest drilling efficiency with no obvious anomalies, making it the most ideal operational condition. It indicates effective drilling that requires minimal intervention.

Slowing-down Drilling: This state is characterized by a significant and sustained decline in the drilling rate (v), specifically a decrease of more than 50% from its stable-stage average, which may occur alongside or precede a stop in rotation. Although drilling continues, the sharp reduction in rate signals a potential obstacle or problem. It necessitates adjusting drilling parameters and closely monitoring conditions to detect and prevent further deterioration.

Intermittent Jamming: This condition occurs when the bit encounters significant obstacles, resulting in an inability to continuously rotate or feed. It is quantitatively characterized by a drop in drilling speed (v) to near zero (<0.1 mm/s) accompanied by a transient spike in torque (T) exceeding 150% of its preceding stable value. This jamming, potentially caused by high rock hardness, insufficient cutting force, or bit wear, leads to a sudden increase in torque, reduced drilling efficiency, and heightened operational risk.

Pipe Sticking: In this critical state, drilling halts completely and cannot continue. It is defined by both the drilling speed (v) and rotational speed (n) remaining at zero for a prolonged period (>10 s) despite applied pressure and torque. This requires the immediate stoppage of equipment to mitigate further risk and potential damage.

The thresholds for defining these four drilling conditions were derived from a quantitative analysis of experimental data trends (Figures 2–4). These experimentally derived, parameter-based criteria were applied by domain experts to annotate the field data sequences, with time-series segments labeled according to the set of criteria they predominantly matched.

4. Principles of Machine Learning Algorithms

4.1. Support Vector Machine

The support vector machine (SVM) is a classification algorithm based on statistical learning theory [20]. Its core principle involves finding the optimal balance between model complexity and generalization ability with limited sample data, which is primarily achieved through the VC dimension theory and the principle of structural risk minimization. To prevent overfitting, the SVM maximizes the distance between the classifier and the training data. Specifically, an SVM consists of support vectors and a hyperplane. By adjusting these parameters, the model can enhance generalization while maintaining classification accuracy [21].

Training data set $A = \{(x_1, y_1), (x_2, y_2) \cdots (x_m, y_m)\}$ comprises m sample points, each containing multiple feature attributes and their corresponding target values or labels. Here, $x_i \in \mathrm{R}$ denotes the i-th feature vector associated with the corresponding $y_i \in \{+1, -1\}$ label. When extending support vector machines from two-dimensional to multi-dimensional sample spaces, Equation (2) can be employed to achieve hyperplane partitioning:

$$\begin{cases} \omega^{\mathrm{T}} \boldsymbol{x}_i + b \geq 0, y_i = +1 \\ \omega^{\mathrm{T}} \boldsymbol{x}_i + b < 0, y_i = -1 \end{cases} \tag{2}$$

$\boldsymbol{\omega}^{\mathrm{T}} \boldsymbol{x}_i + b \geq 0$, the classified samples were divided into positive classes; $\boldsymbol{\omega}^{\mathrm{T}} \boldsymbol{x}_i + b < 0$ is divided into negative categories. Multiplying both sides of the above formula by i yields

$$y_i \left(\boldsymbol{\omega}^{\mathrm{T}} x_i + b \right) \geq 1 \tag{3}$$

$y_i (\boldsymbol{\omega}^{\mathrm{T}} x_i + b) = 1$, that is, the sample point is located on the boundary of the maximum interval.

To ensure accurate classification of all samples, the SVM problem can be transformed into a convex quadratic programming problem [22]:

$$\min \frac{1}{2} \|\omega\|^2 + C \sum_{i=1}^{m} \xi_i \tag{4}$$

The constraint is

$$y_i \left(\omega^{\mathrm{T}} x_i + b \right) \geq 1 - \xi_i, \ \xi_i \geq 0, \ i = 1, 2 \ \ldots, m \tag{5}$$

In the formula, w is the normal vector of the hyperplane, b is the offset constant, C is the penalty coefficient, and ξ_i is the relaxation variable.

4.2. Convolutional Neural Network Algorithms

CNNs are widely used deep learning models [23], primarily composed of convolutional layers, pooling layers, and fully connected layers. The CNN architecture is illustrated in Figure 5. Convolutional layers and pooling layers perform feature engineering, while fully connected layers perform feature weighting. Convolutional layers extract local features and reduce the original data dimensionality through convolution operations; pooling layers perform feature dimensionality reduction by removing partial features; fully connected layers act as the "classifier" of the CNN. For fully connected layers, multiple activation functions are available, and this study adopts the rectified linear unit (ReLU) [24] as the activation function due to its computational simplicity and convergence advantages. The essence of CNNs lies in constructing multiple feature extractors to derive diverse feature vectors or feature maps from large-scale input data. As a deep feed forward network, CNNs are commonly used to process time series, images, and audio data.

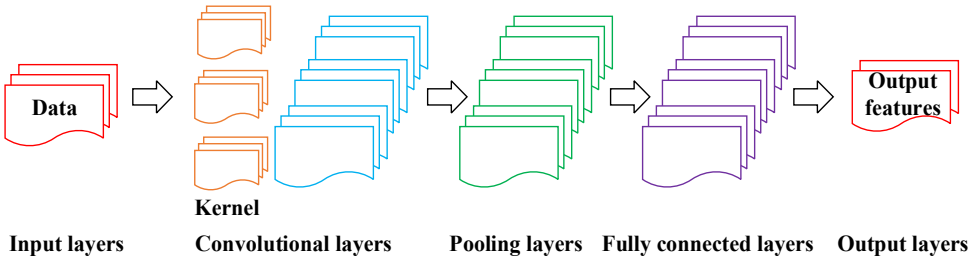


Figure 5. Convolutional neural network architecture.

4.3. Long-Term and Short-Term Memory Network Algorithms

Recurrent neural networks (RNNs) are specialized models designed for processing time-series data [25] and incorporate the concept of "time" to retain information from past periods. Long short-term memory networks (LSTMs), a specialized architecture proposed to address the gradient explosion or vanishing problem in RNNs [26,27], can extract information not only from individual data points but also from entire data series. They have been successfully applied in time-series data processing tasks such as handwritten character recognition, speech recognition, and machine translation. The memory units in an LSTM feature both long-term and short-term memory mechanisms. During neural network training, long-term memory accumulates accumulated training experience through parameter updates at longer intervals, while short-term memory stores historical information in hidden states h, with parameters updated at each time step. LSTM networks overcome numerous limitations of RNNs and have gradually replaced classical recurrent neural networks. The LSTM architecture primarily consists of three gates: the forgetting gate (f_t), input gate (i_t), and output gate (o_t), as illustrated in Figure 6. The forgetting gate (f_t) determines how much of the previous time step's unit state is retained in the current time step's unit state; the input gate (i_t) decides how much of the current time step's input is retained in the current time step's unit state; and the output gate (o_t) specifies how much of the current time step's unit state is output.

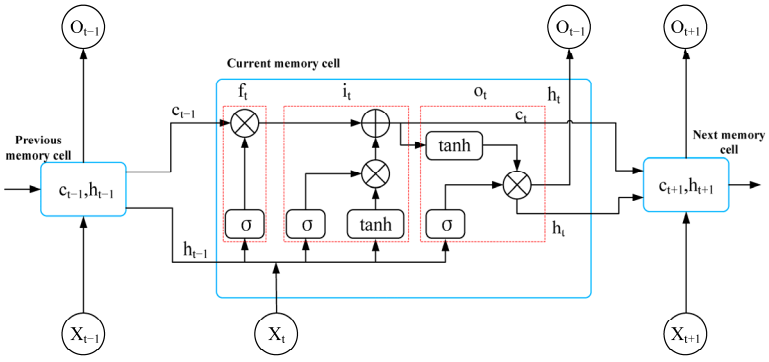


Figure 6. Long short-term memory network architecture.

5. Data and Modeling

5.1. Data

For the purpose of developing and benchmarking data-driven recognition models, this study focuses on the four most frequent and data-rich conditions encountered in field operations: stable drilling, slowing-down drilling, intermittent jamming, and pipe sticking. The micro-drilling experiments provided fundamental insights into the characteristic motion signatures under controlled, scaled conditions. Field data from the Anhui coal mine were used to train and validate the models under realistic operational variability. This approach ensures the model's applicability to similar underground coal mine drilling scenarios. The

training and test datasets were derived from operational parameters of a 5000-sample drill hole collected during underground drilling operations at a coal mine in Anhui Province. Selected sample data are presented in Table 4. During drilling operations, environmental interference may cause abnormal fluctuations in the automatic drilling rig's control system, necessitating outlier detection. The Z-Score method [28] was applied to each sensor channel (torque, drilling speed, rotational speed, drilling pressure). Data points with an absolute Z-Score > 3 in any channel were removed. This process identified and removed 198 samples (approximately 4% of the initial dataset), which were distributed across various drilling depths and did not disproportionately belong to any single predefined condition class (stable, slowing-down, etc.). This cleaning step removed physically implausible sensor spikes likely caused by transient electronic noise, thereby improving the signal quality for model training and preventing the models from learning these artefacts.

Table 4. Partial sample data.

Depth (mm)	Torque (N·m)	Drilling Speed (mm/s)	Rotational Speed (r/min)	Drilling Pressure (N)
200	1429	12	142	47,896
400	1383	12	139	45,341
600	1429	8	141	46,618
800	1459	10	141	51,089
1000	1414	8	139	49,811
1200	1398	8	142	49,811
1400	1505	8	140	47,257
1600	1520	10	139	49,811
1800	1505	12	139	47,896
2000	1368	12	139	49,173
2200	1444	10	139	48,534
2400	1414	8	140	44,703
2600	1398	12	138	44,703
2800	1398	8	139	49,173

The data are normalized to the [0,1] range using the Min-Max normalization method [29] (Equation (2)). The normalized data are then divided into an 80% training set and a 20% test set.

$$x_i' = \frac{x_i - \min(X)}{\max(X) - \min(X)} \tag{6}$$

In the formula, the normalized result is x'_i, the original data are x_i, and the min(X) and max(X) represent the minimum and maximum values of the corresponding data, respectively.

To improve recognition accuracy, time-domain features such as torque and drilling speed are employed as feature indicators, including statistical properties such as mean, root mean square (RMS), variance, standard deviation, skewness, kurtosis, and waveform factor. Here, skewness (γ_1) and kurtosis (γ_2) are mathematically defined as follows:

$$\gamma_1 = \frac{\sum_{i=1}^{N} (x(i) - y_1)^3}{(N-1)y_2^3} \tag{7}$$

$$\gamma_2 = \frac{\sum_{i=1}^{N} (x(i) - y_1)^4}{(N-1)y_2^4} \sum_{i=1}^{n} X_i \tag{8}$$

where, y_1 is the mean, y_2 is the standard deviation, and $x(i)$ represents the data. Note that kurtosis is given in its excess form, where a normal distribution has a value of 0. Additionally, since the selected dataset is time-series ordered, a fixed rolling window of 30 consecutive data points was used, with a step length of 20. This window size was chosen to capture short-term dynamics indicative of transitional drilling states, while remaining small enough to preserve temporal resolution.

By integrating collective statistics and rolling statistics, the system can describe data at various scales, providing more comprehensive information and adapting to more complex and dynamic real-world scenarios. The selected feature indicators include mean and root mean square values for torque and drilling speed, skewness, variance, standard deviation, skewness, waveform factor, rolling average, rolling standard deviation, and first-order difference, totaling 20 feature indicators.

5.2. Recognition Model with SVM

During the construction of the SVM model, the collected torque and drilling speed data undergo multiprocessing to extract multiple feature indicators containing both aggregate and rolling statistical characteristics, followed by normalization. Subsequently, the mutual information method [30] is applied to identify the three most influential features (torque, drilling speed, and skewness) from these indicators, which are then fed into the SVM model for training.

Kernel functions significantly influence the classification outcomes of support vector machines. By selecting appropriate kernel functions, models that are difficult to classify effectively in the original space can be mapped to high-dimensional feature spaces, thereby improving classification accuracy [31]. To evaluate the classification accuracy of different kernel functions, input feature signals were prepared. For each of the three drilling conditions (stable, slowing-down, and intermittent jamming), a distinct subset of data samples was used. The SVM model was then trained and tested using these condition-specific data subsets. The results are presented in Table 5.

Table 5. Accuracy of SVM with different kernel functions.

Kernel Function	Test Accuracy (%)
Sigmoid kernel function	63.3
Radial basis function	66.7
Polynomial kernel function	56
Linear kernel function	33.3

The test results show that the RBF function has the highest accuracy of 66.7%, so the RBF function is selected as the kernel function [32], as shown in Equation (9).

$$\kappa(x_i, x_j) = \exp\left(-g\|x_i - x_j\|^2\right), g > 0 \quad (9)$$

Equations (5) and (9) reveal that the SVM-based drilling condition recognition model incorporates two hyperparameters: C and g. The penalty function C reflects the SVM model's tolerance for misclassification. A higher C value reduces tolerance for misclassification, causing the model to adopt a hard-sigmoid behavior, which may lead to overfitting in practical applications. Conversely, a lower C value increases tolerance for misclassification, sacrificing classification accuracy to enhance the model's robustness against interference.

The parameter g of a radial basis function (RBF) determines its radial coverage. When g exceeds the distance between training data points, the kernel function approaches zero, causing the SVM model to overlearn the current data and resulting in overfitting that

compromises classification accuracy. Conversely, if g is smaller than the distance between data points, the kernel function approaches 1, leading the model to favor the class with more samples.

The selection of penalty function C and kernel function parameter g affects both the classification accuracy and generalization performance of the SVM model. Therefore, a grid search method is employed to optimize the parameter set (C, g) to achieve optimal model performance.

The grid search method is fundamentally an exhaustive algorithm. It begins by generating parameter combinations (C, g) through permutations of the penalty function C and kernel function parameters within the solution space. These combinations are then evaluated to assess their impact on model performance, with the optimal parameters being retained. The optimization process for parameter combinations (C, g) is illustrated in Figure 7.

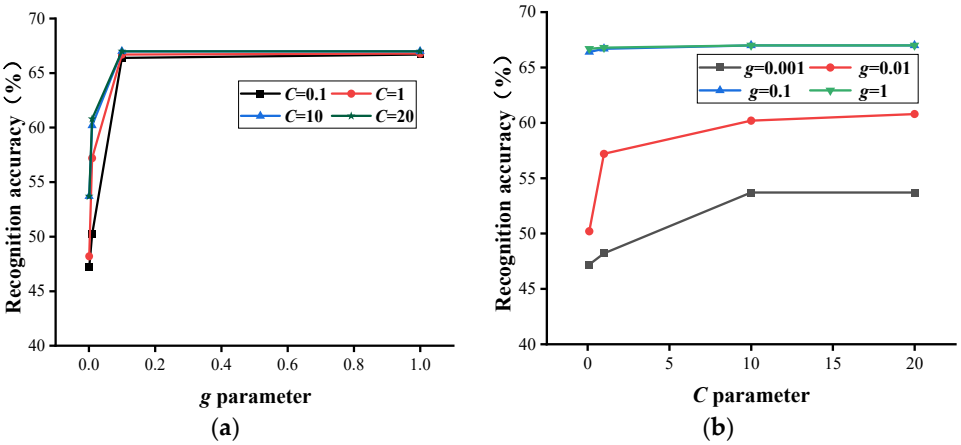


Figure 7. The impact of different hyperparameters on identification accuracy: (**a**) The impact of C on recognition accuracy; (**b**) The impact of g on recognition accuracy.

As shown in Figure 7, parameters C and g significantly influence recognition accuracy, with both showing positive correlations. When g > 0.1, the accuracy remains largely unchanged. Similarly, when C > 10, the accuracy also shows minimal variation. The highest accuracy of 66.7% is achieved when C = 20 and g = 0.1.

5.3. Recognition Model with CNN

The input layer of the CNN model contains three neurons, which correspond to the three main features of torque T and drilling speed v after feature selection. These three main features are input into the recognition model as a one-dimensional array.

The original drilling parameters T and v are normalized through the input layer of the CNN (CNN) and then output to the convolutional layer. The input data of the original drilling parameters are convolved with multiple convolutional kernels to generate feature maps. Input data sequence $X = [x_1, x_2, \ldots, x_N]$; here, N denotes the sequence length. The convolution operation in the convolutional layer is defined as the product of the convolution kernel W ($W \in R^L$) and the concatenated vector $X_{i,j+L-1}$ [33].

$$X_{i,i+L-1} = x_i \oplus x_{i+1} \oplus \wedge \oplus x_{i+L-1} \tag{10}$$

In this formula, $X_{i,j+L-1}$ denotes the sequence signal window starting from the i-th point, where L represents the convolution kernel size, and the $\oplus$ symbol indicates serial connection of data samples.

The convolution operation in the CNN model is defined as follows:

$$z_j^i = W \oplus x_{i,j+L+1} + b = \sum_{i,j} w_j^i x_i + b \tag{11}$$

In this formula, z_j^i denotes the feature learned by the convolution kernel W on the sequence $X_{i,j+L-1}$; w_j^i represents the i-th weight of the j-th convolution kernel; and b is the bias term.

By sliding the convolution kernel from the first to the last sample data point, the feature mapping of the *j*-th convolution kernel can be obtained:

$$z_j^i = \left[z_j^1, z_j^2, K, z_j^{N-L+1}\right] \tag{12}$$

After convolution, ReLU is used as the activation function to activate neurons. The formula of ReLU is described as follows:

$$\alpha_j^i = \sigma\left(z_j^i\right) = \max\left\{0, z_j^i\right\} \tag{13}$$

In this formula, z_j^i denotes the i-th output value generated by the j-th convolution kernel, while α_j^i represents the activation value derived from z_j^i through an activation function.

The pooling layer employs the max-pooling method to reduce the dimensionality of feature maps after convolution operations, extracting key local features. The fully connected layer integrates these dimension-reduced features from the pooling layer and flattens the output of the final pooling layer into a one-dimensional feature vector, which serves as input for subsequent fully connected layers. This establishes a fully connected network between the pooling layer and the output layer. The forward propagation formula for the fully connected layer is

$$z^{(l+1)(j)} = \sum_{i=1}^{n} W_{ij}^l \alpha^{l(i)} + b_j^l \tag{14}$$

In the formula: W_{ij}^l represents the weight between the i-th neuron in layer l and the (l + 1)-th neuron; $z^{(l+1)(j)}$ denotes the logit value of the j-th output neuron in layer (l + 1); b_j^l indicates the bias value of all neurons in layer l toward the j-th neuron in layer (l + 1).

The model training was conducted with 20 epochs using the Adam optimization algorithm, a dropout rate of 0.2, and batch size of 100. Batch normalization was applied to both convolutional and fully connected layers to ensure the model's nonlinear representation capability and accelerate training. The details of the CNN architecture are as shown in Table 6.

Table 6. Architectures and Hyperparameters of the CNN Model.

Component/Hyperparameter	CNN Model
Number of Conv Layers	3
Conv Layer 1	Filters: 32
Conv Layer 2	Filters: 64
Conv Layer 3	Filters: 32
Pooling Layer	Max Pooling (size = 2) + GAP
Classifier Head	3
Dense Layer 1 Units	128
Dropout Rate	0.5
Output Layer Units	of Classes
Activation (Output)	Softmax

Table 6. *Cont.*

Component/Hyperparameter	CNN Model
Training Hyperparameters	
Optimizer	Adam
Initial Learning Rate	0.001
Batch Size	32
Number of Epochs	100
Loss Function	Categorical Cross-entropy

5.4. Recognition Model with LSTM

To construct a typical drilling condition recognition model based on LSTM, the neural information is first simplified through the forgetting gate. The three gates are calculated using the previous external state h_{t-1} and the current input x_t, as shown in Equations (15)–(17) [34].

$$f_t = \sigma\left(W_t[h_{t-1}, x_t] + b_f\right) \tag{15}$$

$$i_t = \sigma(W_i[h_{t-1}, x_t] + b_i) \tag{16}$$

$$\widetilde{c}_t = R_{\mathrm{L}}\left(W_g[h_{t-1}, x_t] + b_g\right) \tag{17}$$

In this formula, R_{L} represents the value of the ReLU function.

The memory unit c_t is updated by integrating the forgetting gate f_t and input gate i_t, then scaled to $[-1, 1]$ using ReLU, and finally synchronized to the external state h_t via the output gate o_t, as shown in Equations (18)–(20).

$$o_t = \sigma(W_o[h_{t-1}, x_t] + b_o) \tag{18}$$

$$c_t = f_t \times c_{t-1} + \widetilde{c}_t \times i_t \tag{19}$$

$$h_t = R_{\mathrm{L}} c_t o_t \tag{20}$$

The input neuron number is 3, the corresponding torque and drilling speed are the data sequence of three parameters after feature selection, the drilling data sequence is mined by multi-layer LSTM structure, the feature is extracted, the data dimension is integrated by the fully connected layer, and the typical drilling condition probability value is output in the output layer.

The core parameters of LSTM directly influence model performance. LSTM comprises three key parameters: sequence length n1, number of hidden layer neurons n2, and number of hidden layers n3.

The greater the number of sequences, the longer the data sequences input to the model, and the more geological information they contain. However, since the increase in sequence count does not always correlate positively with model performance, excessive sequences can lead to oversized parameter sizes, which may slow down model execution. Increasing the number of neurons in the hidden layer enhances model complexity, while adding hidden layers increases the model's nested structure. These two approaches can improve the model's nonlinear fitting capability. However, when the model input is fixed, both methods carry a certain risk of overfitting.

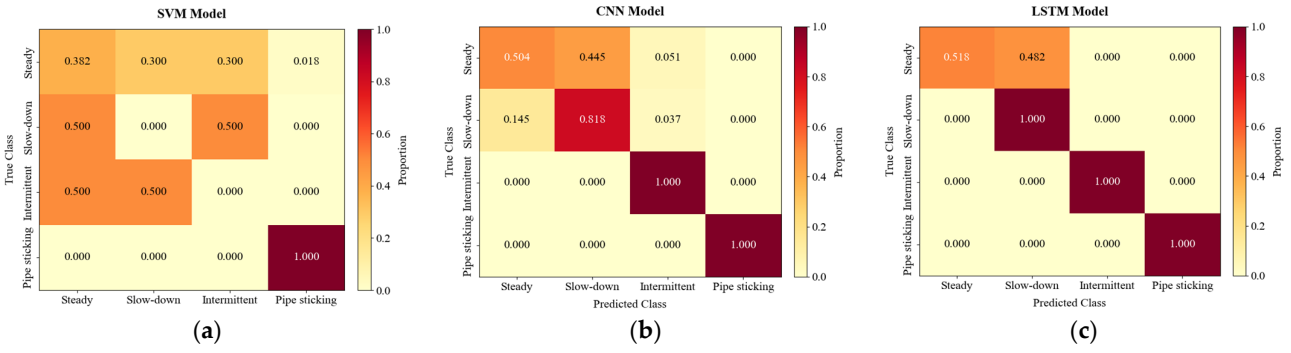
To facilitate comparison of recognition performance across models, the training process was configured with 20 epochs (similarly to CNN models), employing the Adam optimization algorithm with a 0.2 dropout rate. Batch training was implemented using batch size 100, with cross-entropy loss function and batch normalization applied. The details of the LSTM architecture are as shown in Table 7.

Table 7. Architectures and Hyperparameters of the LSTM Model.

Component/Hyperparameter	LSTM Model
Convolutional/Recurrent Layers	2
Layer 1	Units: 64 Return Sequences: True Dropout: 0.2 (Recurrent)
Layer 2	Units: 32 Return Sequences: False Dropout: 0.2 (Recurrent)
Dense Layer Units	64
Dropout Rate (Dense)	0.5
Output Layer Units	# Classes
Activation (Output)	Softmax
Optimizer	Adam
Initial Learning Rate	0.001
Batch Size	32
Number of Epochs	100
Early Stopping Patience	20
Loss Function	Categorical Cross-entropy

5.5. Comparison of Recognition Results

As shown in Figure 8, based on a direct comparative analysis of the row-normalized confusion matrices, the three models exhibit a clear evolutionary progression in their classification behavior and error patterns. The SVM model demonstrates a failure to recognize the 'Slow-down drilling' and 'Intermittent jamming' classes, as all samples from these categories are scattered across other predictions. The CNN model shows significant improvement by achieving perfect classification for two classes but reveals a core weakness in the pronounced bidirectional confusion between the major 'Steady drilling' and 'Slow-down drilling' categories. In stark contrast, the LSTM model presents a near-optimal decision pattern, resolving most of the CNN's confusion and yielding a clean, diagonal matrix where the only significant error is a unidirectional misclassification from 'Steady' to 'Slow-down' drilling. This visual progression directly illustrates the superior capability of the LSTM architecture for this sequential classification task.



(**a**) (**b**) (**c**)

Figure 8. Confusion matrix with different models: (**a**) SVM; (**b**) CNN; (**c**) LSTM.

After model training, the test set was fed into three typical drilling condition recognition models based on CVM, CNN, and LSTM, with the recognition accuracy rates shown in

Table 8. Figure 9 reveals that the recognition accuracy of models based on SVM, CNN, and LSTM varies across different operating conditions. The SVM-based model achieves 42.11% accuracy for condition 1 but shows zero accuracy for conditions 2 and 3. The CNN-based model demonstrates 100% accuracy for condition 3, while its performance for conditions 1 and 2 is 52% and 87.2%, respectively, outperforming the SVM model. The LSTM-based model achieves 100% accuracy for both conditions 2 and 3, and 53% for condition 1, with single condition and sorting recognition accuracy being the highest. A comprehensive comparison of these models indicates that LSTM delivers the best recognition performance.

Table 8. Accuracy of different algorithms.

Algorithm	Steady Drilling	Slowing-Down Drilling	Intermittent Jamming	Pipe Sticking	Average
SVM	42.11%	0%	0%	100%	67.11%
CNN	52%	87.2%	100%	100%	84.8%
LSTM	53%	100%	100%	100%	88.25%

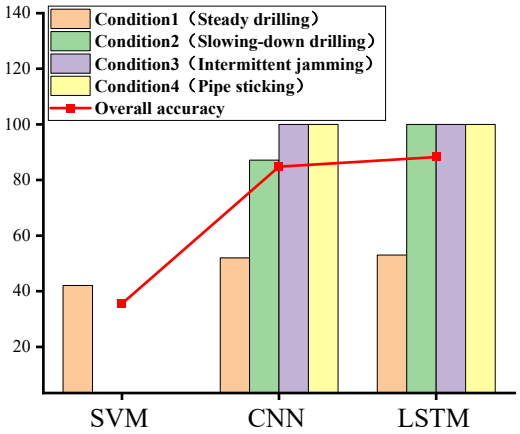


Figure 9. Prediction accuracy results.

In addition, the analysis of the drilling process and the input signal of the model shows that the drilling speed and the intermittent jamming have significant parameter changes, so the recognition accuracy of these two working conditions is high, while the parameters of the stable drilling condition are relatively stable and there is no drastic fluctuation, so the recognition accuracy is low.

A comprehensive comparison of these models indicates that LSTM delivers the best overall recognition performance across all metrics, as summarized in Tables 9–12. An analysis of both recall and precision reveals a consistent performance hierarchy (LSTM > CNN > SVM) and provides deeper insight into model behavior. The LSTM achieves perfect precision and recall (100%) for the three anomalous states ('Slowing-down drilling', 'Intermittent jamming', and 'Pipe sticking'), indicating its predictions for these conditions are both highly reliable (few false positives) and comprehensive (few false negatives). However, for the 'Steady drilling' class, both its recall (51.9%) and precision (49.67%) are substantially lower.

Table 9. Class-wise Recall of different algorithms.

Algorithm	Steady Drilling	Slowing-Down Drilling	Intermittent Jamming	Pipe Sticking	Average
SVM	38.2%	0%	0%	100%	34.55%
CNN	50.4%	81.7%	100%	100%	83.03%
LSTM	51.9%	100%	100%	100%	87.98%

Table 10. Class-wise Precision of different algorithms.

Algorithm	Steady Drilling	Slowing-Down Drilling	Intermittent Jamming	Pipe Sticking	Average
SVM	40.28%	0%	0%	100%	35.09%
CNN	46.75%	84.10%	100%	100%	82.71%
LSTM	49.67%	100%	100%	100%	87.42%

Table 11. Class-wise F1-Score of different algorithms.

Algorithm	Steady Drilling	Slowing-Down Drilling	Intermittent Jamming	Pipe Sticking	Average
SVM	39.23%	0%	0%	100%	34.81%
CNN	48.56%	82.93%	100%	100%	82.87%
LSTM	50.78%	100%	100%	100%	87.69%

Table 12. Macro-performance comparison of different algorithms.

Model	Accuracy	Recall	F1-Score
SVM	35.53%	34.55%	34.81%
CNN	84.8%	83.03%	82.87%
LSTM	88.25%	87.98%	87.69%

This specific performance pattern for 'Steady Drilling' can be attributed to the inherent characteristics of the drilling process. During stable drilling, parameters exhibit small-amplitude, high-frequency fluctuations due to normal heterogeneity in the coal seam. These fluctuations can produce transient signal patterns that superficially resemble the onset of "Slowing-down Drilling" or "Intermittent Jamming". Consequently, the model, trained to be sensitive to such patterns as indicators of anomalies, sometimes generates false positives (lowering precision) for these conditions, while also failing to identify some true 'Steady' states that exhibit ambiguous signals (lowering recall). In contrast, the two anomalous conditions present more pronounced, sustained, and distinctive signal signatures, e.g., a severe and sustained drop in speed, or a sharp torque spike, making them easier for the model to identify with high confidence, as reflected in their perfect recall.

6. Conclusions

(1) A classification system for typical drilling conditions was proposed, based on drilling bit motion characteristics. Four distinct conditions—steady drilling, slowing-down drilling, intermittent jamming, and stuck bit—were defined according to the two primary motion features.

(2) Based on feature engineering, the torque and drilling speed variation characteristics under three sets of parameters were compared and analyzed. The time-domain characteristics of torque and drilling speed were adopted as feature indicators. By combining collective statistical characteristics with rolling statistical characteristics, the comprehensiveness of the data was enhanced, and the accuracy and adaptability of the recognition model were improved.

(3) Three distinct drilling condition recognition models were developed using support vector machines, CNNs, and LSTM. Feature data were input to evaluate their performance, with the LSTM-based model achieving 100% accuracy in detecting slowing-down drilling and intermittent jamming conditions, while maintaining an overall accuracy of 84%—the highest among all models.

(4) The model was developed and validated primarily on data from a specific coal seam geology. Its generalizability to other rock types needs further investigation. Future

work will focus on exploring more advanced deep learning models that may further improve feature extraction and accuracy rate.

Author Contributions: Conceptualization, H.C., Q.W., J.D., Z.W. and L.S.; Methodology, H.C., Q.W., D.X., J.D. and Y.Z.; Validation, H.C., M.S., D.X. and J.D.; Formal analysis, M.S. and L.S.; Investigation, H.C., J.D. and Y.Z.; Resources, M.S.; Data curation, Y.Z.; Writing—original draft, H.C. and Y.Z.; Writing—review and editing, Q.W., M.S., J.D., Z.W. and L.S.; Visualization, D.X.; Supervision, J.D., Z.W. and L.S.; Project administration, Z.W.; Funding acquisition, J.D. All authors have read and agreed to the published version of the manuscript.

Funding: This work was supported by Open Funding of the State Key Laboratory of Coal Mine Disaster Prevention and Control, grant number 2024SKLKF10, funder Jianbo Dai; the National Natural Science Foundation of China, grant number 52404179, funder Jianbo Dai; Special Fund for Technological Innovation and Entrepreneurship of Tian Di Science and Technology Co., Ltd., grant number 2024-TD-QN004, funder Hang Chen.

Data Availability Statement: The data presented in this study are available on request from the corresponding author.

Conflicts of Interest: Authors Hang Chen, Qingfeng Wang, and Dezhong Xin were employed by the company CCTEG Chongqing Research Institute Co., Ltd. The remaining authors declare that the research was conducted in the absence of any commercial or financial relationships that could be construed as a potential conflict of interest. The authors declare that this study received funding from Technological Innovation and Entrepreneurship of Tian Di Science and Technology Co., Ltd. The funder was not involved in the study design, collection, analysis, interpretation of data, the writing of this article or the decision to submit it for publication.

References

1. Kokkinis, A.; Frantzis, T.; Skordis, K.; Nikolakopoulos, G.; Koustoumpardis, P. Review of Automated Operations in Drilling and Mining. *Machines* **2024**, *12*, 845. [CrossRef]
2. Cayeux, E.; Daireaux, B.; Karimi, M.; Haavardstein, S.; Magne Stokland, L.; Saasen, A. Automatic performance analysis and estimation of risk level embedded in drilling operation plans. In Proceedings of the SPE Intelligent Energy International Conference and Exhibition, Aberdeen, UK, 6–8 September 2016.
3. Elmgerbi, A.; Les, B.; Ashena, R.; Atkin, T. A Practical Decision Tool to Evaluate and Rank Potential Solutions for Expected Downhole Drilling Problems During the Well-planning Phase. *J. Inst. Eng. India Ser. D* **2022**, *103*, 25–36. [CrossRef]
4. Zhang, K.; Kang, L.; Chen, X.; He, M.; Zhu, C.; Li, D. A Review of Intelligent Unmanned Mining Current Situation and Development Trend. *Energies* **2022**, *15*, 513. [CrossRef]
5. Li, W.; Chen, S.; Lu, C.; Mu, L.; Yang, A.; Zhang, Y.; Song, H.; Yao, N.; Tian, H.; Wu, M. Equivalent-input-disturbance based rotating control of drill-string in compound directional drilling process subject to coal seam variation. *ISA Trans.* **2025**, *160*, 434–445. [CrossRef]
6. Zhang, W.; Li, C.; Jin, J.; Qu, X.; Fan, S. A new monitoring-while-drilling method of large diameter drilling in underground coal mine and their application. *Measurement* **2021**, *173*, 108840. [CrossRef]
7. Liu, X.; Wang, Q.; Liu, Y. Research on the drilling state intelligent sensing and adaptive optimization control of the fast drilling robot. *J. Phys. Conf. Ser.* **2024**, *2902*, 012045. [CrossRef]
8. Zhang, Y.; Zhang, N.; Liu, P.; Pei, J.; He, B. Study on drilling dynamic characteristics and stratum information identification of anchor hole in typical coal-bearing stratum. *Coal Sci. Technol.* **2021**, *49*, 177–185.
9. Wang, Y.; Zhao, A.; Yu, Z.; Guo, J.; Du, K.; Ma, D. Research and Application of the Deviation Reduction Mechanism in Stratified Cutting Drilling of Soft-Fragmented Coal Seams. *ACS Omega* **2024**, *10*, 1388–1400. [CrossRef]
10. Rosiani, D.; Zulfan; Suranta, B.Y.; Sofyan, A.; Pradana, F.G.; Putra, R.B. Machine Learning Classifies Data for Early Warning of Stuck Pipe Detection in Geothermal Drilling. *Int. J. Adv. Sci. Eng. Inf. Technol.* **2025**, *15*, 44–51. [CrossRef]
11. Sun, T.; Zhao, Y.; Yang, J.; Yin, Q.; Wang, W.; Chen, Y. Real-time Intelligent Identification Method of Drilling Condition Based on Support Vector Machine. *Pet. Drill. Technol.* **2019**, *47*, 28–33.
12. Gao, Y.; Yu, X.; Su, Y.; Yin, Z.; Wang, X.; Li, S. Intelligent Identification Method for Drilling Conditions Based on Stacking Model Fusion. *Energies* **2023**, *16*, 883. [CrossRef]

13. Du, Z. Research on Intelligent Recognition Diagnosis Method of Overflow. Master's Thesis, China University of Petroleum (Beijing), Beijing, China, 2020.
14. Yin, Q.; Yang, J.; Zhou, B. Improve the Drilling Operations Efficiency by the Big Data Mining of Real-Time Logging. In Proceedings of the SPE/IADC Middle East Drilling Technology Conference and Exhibition, Abu Dhabi, United Arab Emirates, 29–31 January 2018.
15. Wang, C.; Liu, G.; Yang, Z.; Li, J.; Zhang, T.; Jiang, H.; Cao, C. Downhole working conditions analysis and drilling complications detection method based on deep learning. *J. Nat. Gas Sci. Eng.* **2020**, *81*, 103485. [CrossRef]
16. Jared, S.; Srikanta, M.; Luan, L.; Chandramohan, D. Ensemble Learning: A Robust Paradigm for Data-Driven Modeling in Unconventional Reservoirs. In Proceedings of the Unconventional Resources Technology Conference, Denver, CO, USA, 22–24 July 2019.
17. Qin, M.; Hu, X.; Liang, Y.; Yuan, W.; Yang, D. Identification of High Temperature and High-Pressure Reservoir Fluid Using Stacking Model Fusion Method. *Oil Geophys. Prospect.* **2021**, *56*, 364–371.
18. Zhao, Y.; Huang, Z.; Xin, F.; Qi, G.; Huang, H. Kick Prediction Method Based on Artificial Neural Network Mode. *Energies* **2022**, *15*, 5912. [CrossRef]
19. Zhou, Z.; Li, S.; Li, X.; Chen, D.; Zheng, B. Evaluation of rock-bit interaction test under simulated ultra-deep well conditions based on similarity principle. *J. Pet. Sci. Eng.* **2022**, *211*, 110130. [CrossRef]
20. Vapnik, V. An overview of statistical learning theory. *IEEE Trans. Neural Netw.* **1999**, *10*, 988–999. [CrossRef]
21. Burges, C.J.C. A tutorial on support vector machines for pattern recognition. *Data Min. Knowl. Discov.* **1998**, *2*, 121–167. [CrossRef]
22. Piccialli, V.; Sciandrone, M. Nonlinear optimization and support vector machines. *Ann. Oper. Res.* **2022**, *314*, 15–47. [CrossRef]
23. LeCun, Y.; Bengio, Y.; Hinton, G. Deep learning. *Nature* **2015**, *521*, 436–444. [CrossRef] [PubMed]
24. Park, Y.; Hwang, G.; Lee, W.; Park, S. Expressive power of ReLU and step networks under floating-point operations. *Neural Netw.* **2024**, *175*, 106297. [CrossRef]
25. Mienye, I.; Swart, T.; Obaido, G. Recurrent Neural Networks: A Comprehensive Review of Architectures, Variants, and Applications. *Information* **2024**, *15*, 517. [CrossRef]
26. Tuhin, K.; Nobi, A.; Rakib, M.; Lee, J. Long short-term memory autoencoder based network of financial indices. *Humanit. Soc. Sci. Commun.* **2025**, *12*, 100. [CrossRef]
27. Narisetty, N.; Babu, K.; Gavarraju, L. Design of an integrated model combining recurrent convolutions and attention mechanism for time series prediction. *J. Supercomput.* **2025**, *81*, 642. [CrossRef]
28. Lee, K.; Kim, T.; Han, S. Robust optimization of rubber domes by using a Z-score and the penalty method. *J. Mech. Sci. Technol.* **2016**, *30*, 4471–4474. [CrossRef]
29. Savitha, K.N.; Pinto, L.; Gopalan, S.; Balasubramaniam, P. Equivalence class and modified Gaussian methods for normalization of time series data on AI models. *Expert Syst. Appl.* **2025**, *277*, 127166. [CrossRef]
30. Liu, G.; Yang, C.; Liu, S.; Xiao, C.; Song, B. Feature Selection Method Based on Mutual Information and Support Vector Machine. *Int. J. Pattern Recognit. Artif. Intell.* **2021**, *35*, 2150021. [CrossRef]
31. Xue, S.; Zhang, L.; Zhu, Z. Design of semi-tensor product-based kernel function for SVM nonlinear classification. *Control Theory Technol.* **2022**, *20*, 456–464. [CrossRef]
32. Luo, L.; Yang, Q.; Peng, H.; Wang, Y.; Chen, Z. MaxMin-L2-SVC-NCH: A novel approach for support vector classifier training and parameter selection. *Neurocomputing* **2025**, *623*, 129438. [CrossRef]
33. Krizhevsky, A.; Sutskever, I.; Hinton, G. ImageNet classification with deep convolutional neural networks. *Adv. Neural Inf. Process. Syst.* **2012**, *25*, 1097–1105. [CrossRef]
34. Hochreiter, S.; Schmidhuber, J. Long short-term memory. *Neural Comput.* **1997**, *9*, 1735–1780. [CrossRef] [PubMed]

Disclaimer/Publisher's Note: The statements, opinions and data contained in all publications are solely those of the individual author(s) and contributor(s) and not of MDPI and/or the editor(s). MDPI and/or the editor(s) disclaim responsibility for any injury to people or property resulting from any ideas, methods, instructions or products referred to in the content.